

Article

Phase Composition and Mechanical Properties of Sm_2O_3 Partially Stabilized Zirconia Crystals

Mikhail Borik¹, Artem Chislov^{1,2}, Alexej Kulebyakin¹ , Elena Lomonova¹ , Filipp Milovich^{1,2,*} ,
Valentina Myzina¹, Polina Ryabochkina³, Nataliya Sidorova³ and Nataliya Tabachkova^{1,2} 

¹ Prokhorov General Physics Institute of the Russian Academy of Sciences, 38 Vavilov Str., 119991 Moscow, Russia

² Department of Materials Science of Semiconductors and Dielectrics, National University of Science and Technology (MISIS), 4 Leninskiy Prospekt, 119049 Moscow, Russia

³ Institute of High Technologies and New Materials, Ogarev Mordovia State University, 68 Bolshevistskaya Str., 430005 Saransk, Russia

* Correspondence: philippmilovich@gmail.com; Tel.: +7-(964)-527-15-71

Abstract: The mechanical properties, phase composition and luminescence of $(\text{ZrO}_2)_{1-x}(\text{Sm}_2\text{O}_3)_x$ ($x = 0.02\text{--}0.06$) crystals synthesized using directional melt crystallization were studied. The regularities of changes in the phase composition of the crystals depending on samaria concentration were analyzed. Optical spectroscopy showed that Sm ions were incorporated into the ZrO_2 crystal lattice in the form of Sm^{3+} . The microhardness of the crystals was shown to increase with Sm_2O_3 concentration and reached 12.45 GPa for $(\text{ZrO}_2)_{0.94}(\text{Sm}_2\text{O}_3)_{0.06}$ crystals. The highest fracture toughness of 14.2 $\text{MPa}\cdot\text{m}^{1/2}$ was observed for the crystals containing 3.7 mol.% Sm_2O_3 . The experimental results were analyzed in order to understand the effect of phase composition on the mechanical properties of the crystals. The effect of ionic radii of stabilizing oxide cations (i.e., Y^{3+} , Gd^{3+} and Sm^{3+}) on the mechanical properties of the materials on the basis of partially stabilized zirconia was also discussed.

Keywords: partially stabilized zirconia; skull melting; solid solutions; mechanical properties



Citation: Borik, M.; Chislov, A.; Kulebyakin, A.; Lomonova, E.; Milovich, F.; Myzina, V.; Ryabochkina, P.; Sidorova, N.; Tabachkova, N. Phase Composition and Mechanical Properties of Sm_2O_3 Partially Stabilized Zirconia Crystals. *Crystals* **2022**, *12*, 1630. <https://doi.org/10.3390/cryst12111630>

Academic Editor: Pavel Lukáč

Received: 18 October 2022

Accepted: 10 November 2022

Published: 13 November 2022

Publisher's Note: MDPI stays neutral with regard to jurisdictional claims in published maps and institutional affiliations.



Copyright: © 2022 by the authors. Licensee MDPI, Basel, Switzerland. This article is an open access article distributed under the terms and conditions of the Creative Commons Attribution (CC BY) license (<https://creativecommons.org/licenses/by/4.0/>).

1. Introduction

Materials based on partially stabilized zirconia (PSZ) exhibit excellent mechanical and friction properties and are resistant to high temperatures and corrosive media. These materials find broad applications as construction materials, thermal barriers and protective coatings, orthopedic and dental implants, solid state electrolytes and solid oxide fuel cells [1–4].

PSZ is recognized as having good mechanical properties, for example, fracture toughness that originates from transformation hardening. The mechanism of transformation hardening is based on a tetragonal to monoclinic phase transition induced by mechanical stress [5,6]. For this reason, the study of phase transformations in $\text{ZrO}_2\text{--R}_2\text{O}_3$ binary systems (R being a rare-earth element) as well as factors affecting the phase composition of zirconia-based solid solutions has attracted great interest from researchers [7–14]. Most of the works published on the topic so far have dealt with yttria-stabilized zirconia. However, of interest are also materials partially stabilized by Nd, Sm, Gd, Dy and Yb oxides. Studies of the phase diagrams of $\text{ZrO}_2\text{--R}_2\text{O}_3$ systems (R being Y, Nd, Sm, Gd, Dy, Yb) have shown that the ZrO_2 -rich side of the diagrams contains not only thermodynamically stable monoclinic (m), tetragonal (t) and cubic (c) phases but also metastable t' and t'' tetragonal ones [15–19]. Under specific conditions of material synthesis, these phases can be retained at room temperature. However, the abovementioned phase diagrams have differences because of the different ionic radii of trivalent stabilizing cations. For example, in binary $\text{ZrO}_2\text{--R}_2\text{O}_3$ systems (R being Y, Gd, Sm, Nd), an increase in the trivalent cation radius shifts the $t/t + c$ phase boundary towards lower stabilizing oxide concentrations, whereas the

t + c/c phase boundary shifts towards higher stabilizing oxide concentrations [16,17]. This causes broadening of the t + c two-phase region where most of the high fracture toughness compositions are located.

We previously studied the structural and mechanical properties of zirconia crystals partially stabilized by yttria or gadolinia [20–22]. Comparison of the structural and mechanical properties of these crystals showed that an increase in the ionic radius of the trivalent cation ($R_{\text{Gd}^{3+}} = 1.053\text{\AA}$, $R_{\text{Y}^{3+}} = 1.019\text{\AA}$) changes the ratio of the metastable tetragonal phases and leads to an increase in the fracture toughness of the material at comparable stabilizing oxide concentrations. Sm^{3+} ions ($R_{\text{Sm}^{3+}} = 1.079\text{\AA}$) are larger than Gd^{3+} ones, and therefore one can expect that the use of Sm_2O_3 as a stabilizing oxide will further improve the mechanical properties of the crystals.

The aim of this work is to carry out melt synthesis of zirconia crystals partially stabilized by samaria and to study the phase composition and mechanical properties of this new material.

2. Materials and Methods

A series of $(\text{ZrO}_2)_{1-x}(\text{Sm}_2\text{O}_3)_x$ ($x = 0.02\text{--}0.06$) crystals were grown using directional melt crystallization from a 130-mm-diam. water-cooled copper crucible. The heater was a high-frequency (5.28-MHz) 60-kW generator. Directional melt crystallization was achieved by lowering the crucible relative to the induction heater at a 10-mm/h speed. Detailed description of zirconia-based crystal growth using this method was published earlier [23]. The raw materials were at least 99.99% purity ZrO_2 and Sm_2O_3 powders. The charge was prepared for melting by mechanical mixing of the raw oxide powders in the required ratio.

The phase composition was studied using X-ray diffraction on a Bruker D8 instrument in $\text{CuK}\alpha$ radiation and Raman spectroscopy on a Renishaw inVia microscope-spectrometer. The luminescence spectra were recorded at 300 K using an FHR 1000 spectrometer (Horiba) and a Hamamatsu R928 photomultiplier as a light detector. The luminescence spectra are presented in relative units ignoring the instrumental spectral sensitivity. The microhardness and fracture toughness of the crystals were measured by microindentation with a DM 8 B AUTO microhardness tester having Vickers indenters and a Wolpert Hardness Tester 930. The microhardness and fracture toughness measurements were carried out at loads of 5 and up to 200 N, respectively. The specimens for the measurements were in the form of polished wafers cut from the middle parts of the crystals oriented in the {100} plane. The indenter diagonals were oriented in the <100> and <110> directions in the specimen plane, the angle between these directions being 45 arc deg. The fracture toughness (K_{1c}) was calculated using the Niihara equation for the Palmqvist crack system [24].

$$K_{1c} = 0.035(L/a)^{-1/2}(CE/H)^{2/5}Ha^{1/2}C^{-1} \quad (1)$$

where K_{1c} is the stress intensity factor ($\text{MPa}\cdot\text{m}^{1/2}$); L is the radial crack length (m); a is the indentation halfwidth (m); C is the constraint factor (=3); E is the Young modulus (Pa); and H is the microhardness (Pa). K_{1c} was calculated for the radial cracks around the indentation, the length of which met the criterion $0.25 \leq l/a \leq 2.5$ for Palmqvist cracks.

3. Results and Discussion

Figure 1 shows photographic images of crystals with different compositions. The crystals had a yellow color with the color intensity increasing with the Sm_2O_3 concentration. Furthermore, the crystals exhibited differences in their surface morphology. For example, the crystals containing 2.0 mol.% Sm_2O_3 (Figure 1a) had a matted rough surface, whereas the surfaces of the crystals containing 2.9 mol.% Sm_2O_3 (Figure 1c) were smooth and semitransparent. The surface morphology of the crystals containing 2.0 mol.% Sm_2O_3 (Figure 1b) varied along the crystal, from the matted bottom part of the crystal to the semitransparent top.

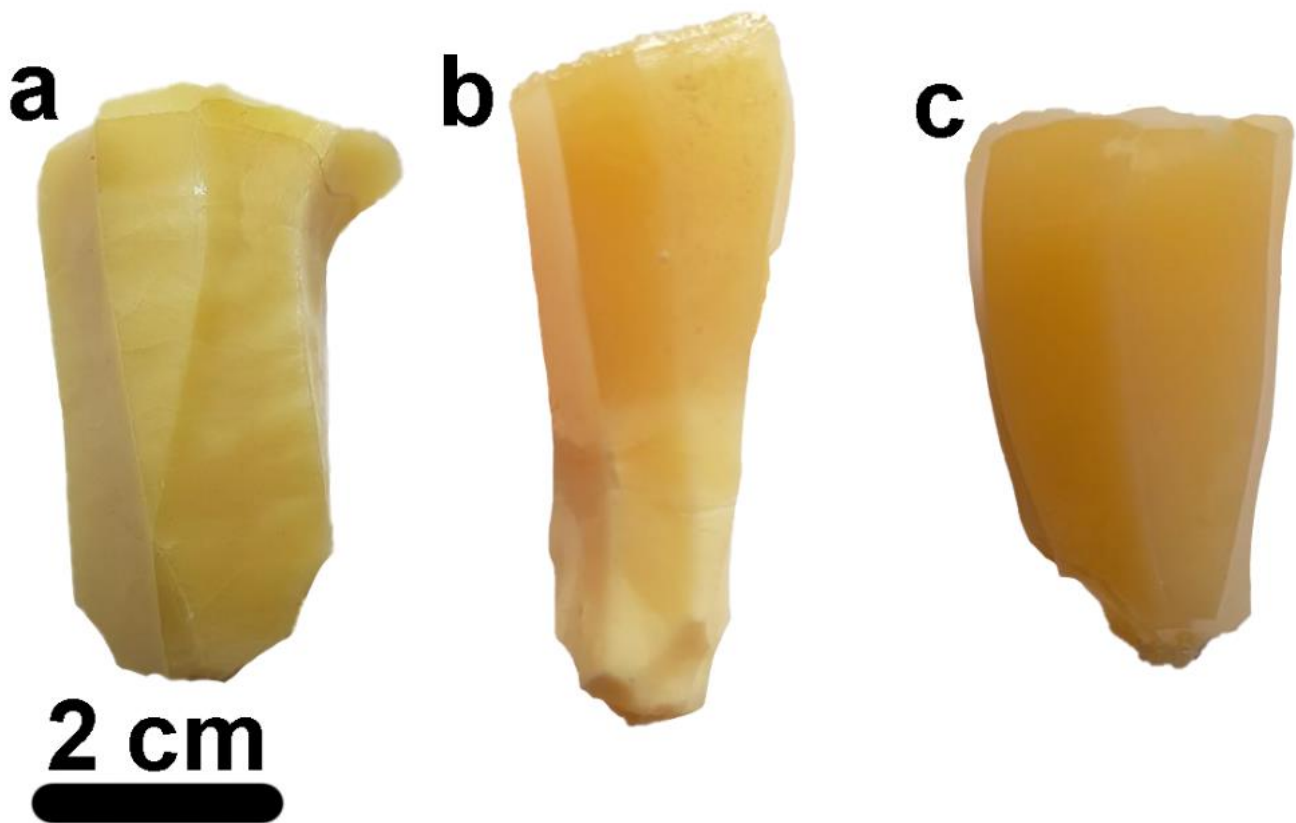


Figure 1. Photographic images of $(\text{ZrO}_2)_{1-x}(\text{Sm}_2\text{O}_3)_x$ crystals: (a) $(\text{ZrO}_2)_{0.98}(\text{Sm}_2\text{O}_3)_{0.02}$, (b) $(\text{ZrO}_2)_{0.97}(\text{Sm}_2\text{O}_3)_{0.03}$ and (c) $(\text{ZrO}_2)_{0.96}(\text{Sm}_2\text{O}_3)_{0.04}$.

An earlier study of ZrO_2 crystals partially stabilized with Y_2O_3 showed that the observed evolution of the appearance and surface morphology of the crystals stems from the difference in the concentration of the stabilizing oxide, which determines the crystalline structure [25]. One can assume that the same is true for the $(\text{ZrO}_2)_{1-x}(\text{Sm}_2\text{O}_3)_x$ crystals. To check this assumption, we carried out a local Raman study of the phase composition at different points of the crystals containing 2, 3 and 4 mol.% Sm_2O_3 (Figure 2).

The spectra of the $(\text{ZrO}_2)_{0.98}(\text{Sm}_2\text{O}_3)_{0.02}$ crystals exhibit monoclinic phase bands and weak tetragonal phase bands along the whole crystal (Figure 2a). The spectra of the $(\text{ZrO}_2)_{0.96}(\text{Sm}_2\text{O}_3)_{0.04}$ crystals (Figure 2c) exhibit tetragonal phase bands only. For a Sm_2O_3 concentration of 3 mol.% (Figure 2b), the monoclinic phase dominates in the bottom part of the crystal, whereas the spectra for the rest of the crystal have patterns similar to those typical of the tetragonal phase [26].

These experimental results suggest a possible composition variation in the length of the crystals, potentially causing errors in the results of further studies. To rule out any composition indeterminacy, we conducted further studies for specimens cut from the middle parts of the test crystals.

Sm cations are known to exist in crystals and glasses in the form of Sm^{3+} and Sm^{2+} [27–29]. To determine the charge state of Sm cations in partially stabilized ZrO_2 , we studied luminescence spectra of the $(\text{ZrO}_2)_{0.96}(\text{Sm}_2\text{O}_3)_{0.04}$ crystals using optical spectroscopy. Figure 3 shows the luminescence spectra of these crystals.

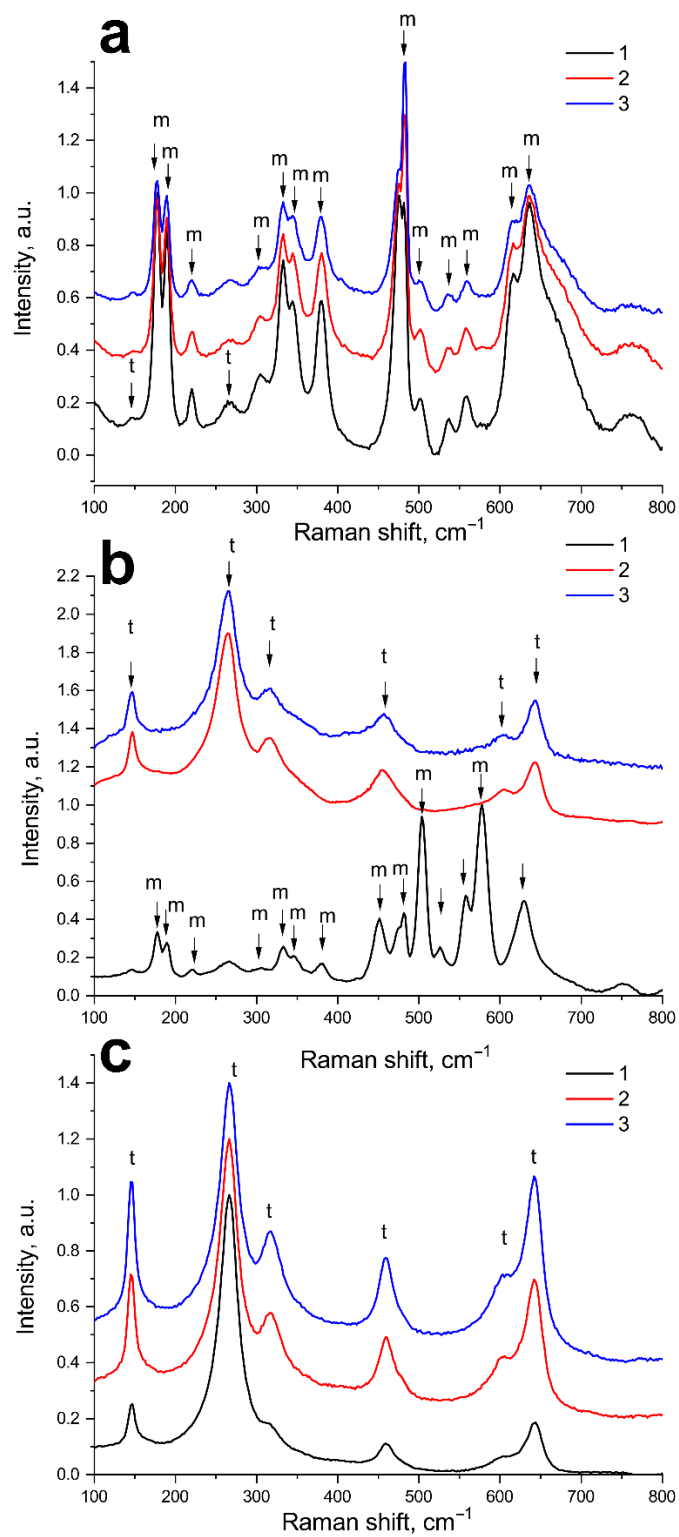


Figure 2. Raman spectra of $(\text{ZrO}_2)_{1-x}(\text{Sm}_2\text{O}_3)_x$ crystals: (a) $(\text{ZrO}_2)_{0.98}(\text{Sm}_2\text{O}_3)_{0.02}$, (b) $(\text{ZrO}_2)_{0.097}(\text{Sm}_2\text{O}_3)_{0.03}$ and (c) $(\text{ZrO}_2)_{0.96}(\text{Sm}_2\text{O}_3)_{0.04}$; (1) crystal bottom, (2) crystal middle part and (3) crystal top.

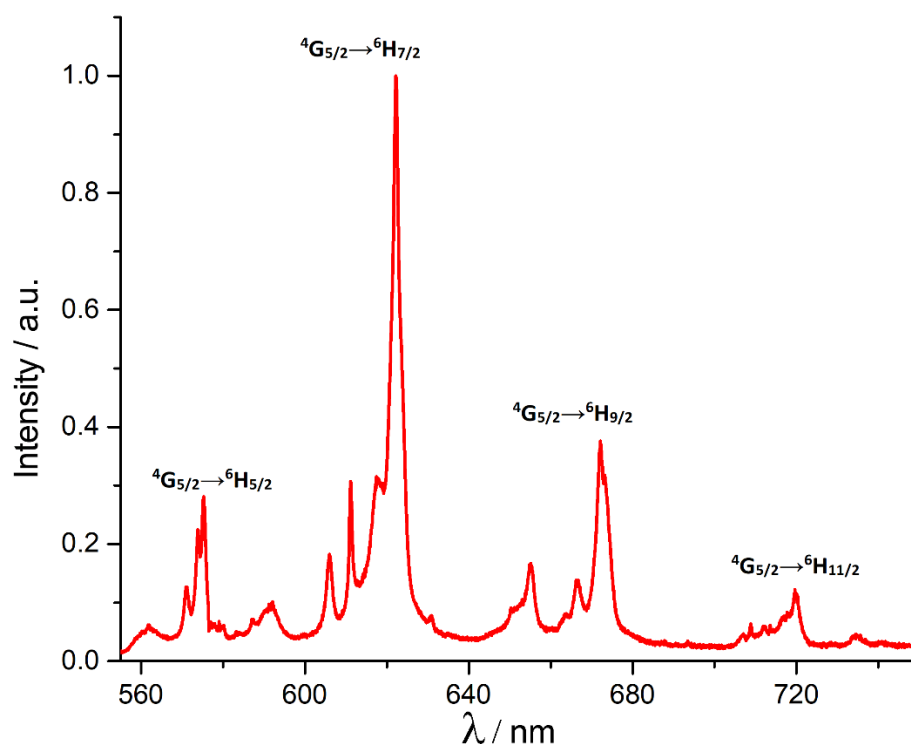


Figure 3. Luminescence spectra of $(\text{ZrO}_2)_{0.96}(\text{Sm}_2\text{O}_3)_{0.04}$ crystals upon excitation to the ${}^4\text{G}_{5/2}$ level of Sm^{3+} ions, $\lambda_{\text{ex}} = 532$ nm.

The luminescence spectra exhibited bands in the green, yellow and red regions, corresponding to the ${}^4\text{G}_{5/2} \rightarrow {}^6\text{H}_{5/2}$, ${}^4\text{G}_{5/2} \rightarrow {}^6\text{H}_{7/2}$ and ${}^4\text{G}_{5/2} \rightarrow {}^6\text{H}_{9/2}$ transitions of Sm^{3+} ions, respectively. However, the spectra did not contain 675–775 nm bands that are typical of Sm^{2+} ions. Annealing of the crystals at 1200 °C in air for 2 h did not cause any visible changes to the luminescence spectra. Thus, Sm cations are mainly present in the ZrO_2 lattice in the trivalent charge state.

X-ray diffraction data for the crystals containing 2.0 mol.% Sm_2O_3 suggest that the crystals contained the monoclinic ZrO_2 modification (Figure 4a). At $2.8 \leq \text{Sm}_2\text{O}_3 \leq 3.2$ mol.% concentrations the crystals contained a mixture of the monoclinic and tetragonal ZrO_2 modifications, the quantity of the monoclinic phase decreasing with an increase in the Sm_2O_3 concentration. The crystals containing $\text{Sm}_2\text{O}_3 \geq 3.7$ mol.% did not contain the monoclinic phase. In the $3.7 \leq \text{Sm}_2\text{O}_3 \leq 6.0$ mol.% concentration range, the X-ray diffraction spectra of the crystals only exhibited reflections of two tetragonal phases differing in the tetragonality degree. Figure 4b shows the X-ray diffraction pattern of the $(\text{ZrO}_2)_{0.96}(\text{Sm}_2\text{O}_3)_{0.04}$ crystal, this pattern being typical of the two other crystals containing only two tetragonal phases.

The crystal lattice parameters and the tetragonality degrees of the crystals containing only two tetragonal ZrO_2 modifications are summarized in Table 1. The t phase has a tetragonality degree of 1.017–1.016, the tetragonality degree of the t' phase being slightly greater than 1. The presence of the metastable tetragonal t phase with a large tetragonality degree in the ZrO_2 - R_2O_3 systems is an indispensable condition determining the good mechanical properties of the materials [5,6]. Due to the ability to undergo a tetragonal to monoclinic phase transformation under mechanical loads, this phase is referred to as transformable. It can be seen from Table 1 that an increase in the Sm_2O_3 concentration leads to a decrease in the content of the transformable t phase and, hence, an increase in the content of the non-transformable phase. It is worth mentioning that an increase in the Sm_2O_3 concentration is also accompanied by a slight decrease in the tetragonality degree of both phases.

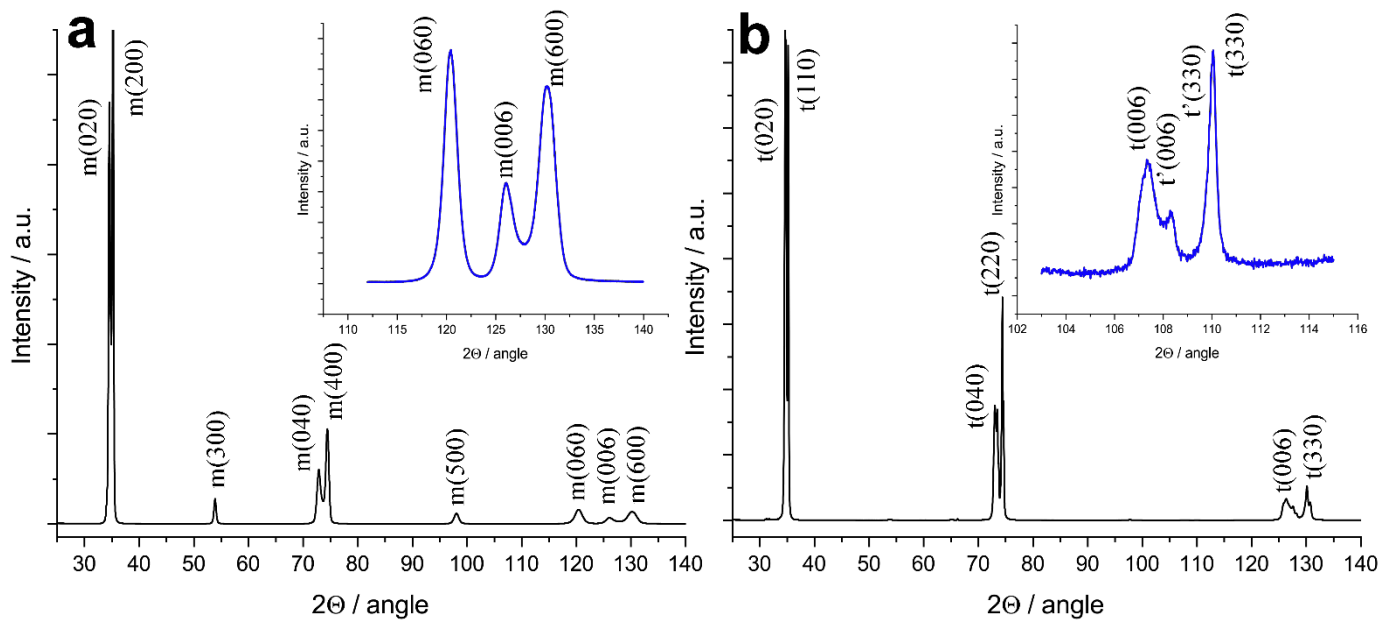


Figure 4. X-ray diffraction patterns of (a) $(\text{ZrO}_2)_{0.98}(\text{Sm}_2\text{O}_3)_{0.02}$ and (b) $(\text{ZrO}_2)_{0.96}(\text{Sm}_2\text{O}_3)_{0.04}$ crystals.

Table 1. Phase composition and lattice parameters in different tetragonal phases of $(\text{ZrO}_2)_{1-x}(\text{Sm}_2\text{O}_3)_x$ crystals.

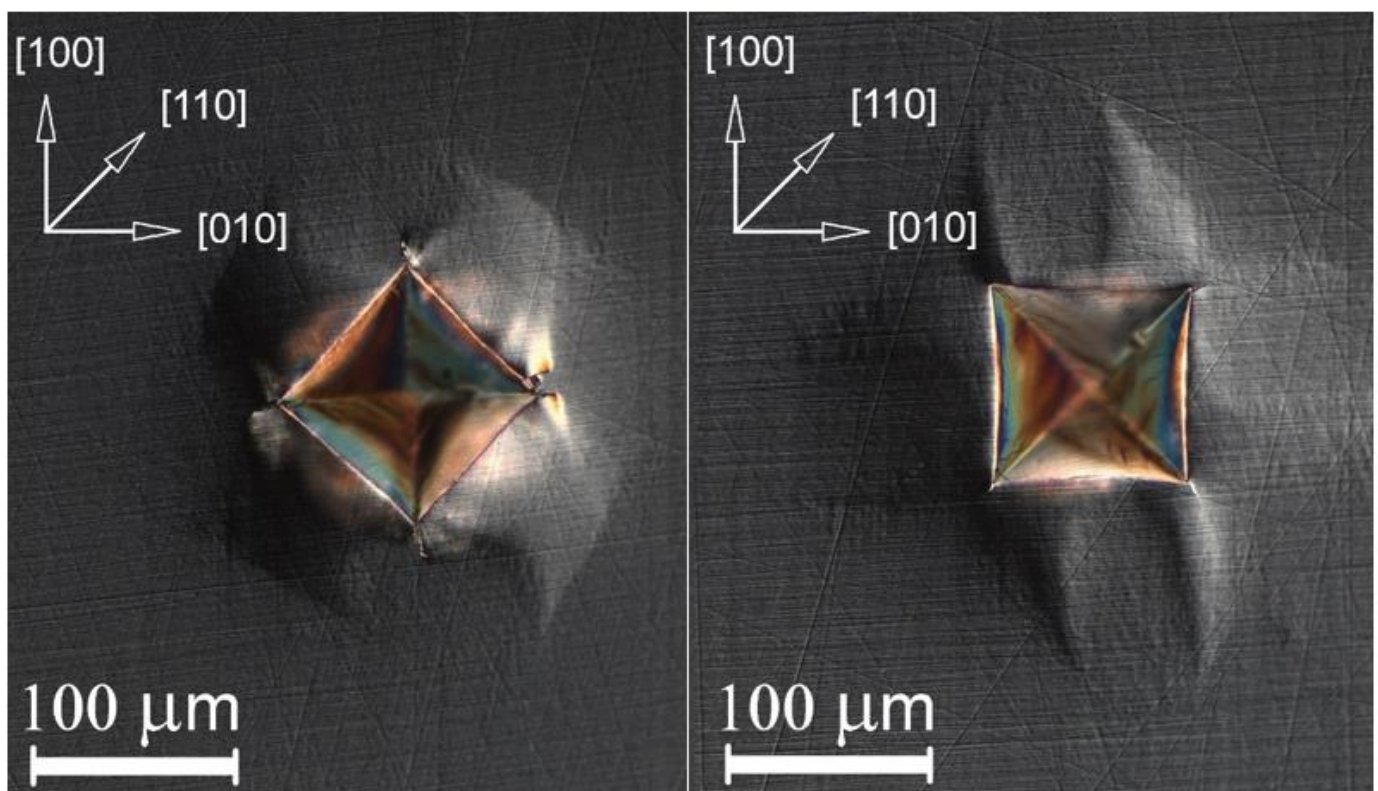
Specimen	Phase	Wt, %	a, Å	c, Å	$c/\sqrt{2a}$
$(\text{ZrO}_2)_{0.963}(\text{Sm}_2\text{O}_3)_{0.037}$	t	85 ± 5	3.6062(1)	5.1866(2)	1.0170
	t'	15 ± 5	3.6426(2)	5.1695(5)	1.0035
$(\text{ZrO}_2)_{0.96}(\text{Sm}_2\text{O}_3)_{0.04}$	t	75 ± 5	3.6063(1)	5.1854(2)	1.0167
	t'	25 ± 5	3.6429(2)	5.1692(5)	1.0134
$(\text{ZrO}_2)_{0.95}(\text{Sm}_2\text{O}_3)_{0.05}$	t	70 ± 5	3.6068(1)	5.1815(2)	1.0158
	t'	30 ± 5	3.6434(2)	5.1683(5)	1.0031
$(\text{ZrO}_2)_{0.94}(\text{Sm}_2\text{O}_3)_{0.06}$	t	60 ± 5	3.6073(1)	5.1767(2)	1.0147
	t'	40 ± 5	3.6438(2)	5.1672(5)	1.0028

Table 2 shows the microhardness and fracture toughness of the $(\text{ZrO}_2)_{1-x}(\text{Sm}_2\text{O}_3)_x$ crystals. The lowest microhardness and fracture toughness are observed in the crystals containing 2.0 and 2.8 mol.% Sm_2O_3 . With an increase in the Sm_2O_3 concentration from 3.0 to 6.0 mol.% the microhardness grows in a monotonic manner. The change in the fracture toughness of the crystals in this concentration range has a more complex pattern. The fracture toughness initially increases, reaching a peak at 3.7 mol.% Sm_2O_3 , and then sees a gradual decline. This behavior of the fracture toughness remains the same for different indenter diagonal orientations, but the fracture toughness for the $\langle 100 \rangle$ indenter diagonal orientation is higher than that for the $\langle 110 \rangle$ orientation.

Figure 5 shows indentations for the $\langle 100 \rangle$ and $\langle 110 \rangle$ indenter diagonal orientations. It can be seen that the indentation produces a surface pile-up in the $\langle 110 \rangle$ direction regardless of indenter diagonal orientation.

Table 2. Microhardness and fracture toughness of $(\text{ZrO}_2)_{1-x}(\text{Sm}_2\text{O}_3)_x$ crystals.

Sm ₂ O ₃ Content, mol.%	Microhardness HV, GPa	Fracture Toughness, MPa·m ^{1/2}	
		<100>	<110>
2.0	8.65 ± 0.30	5.0 ± 0.5	4.0 ± 0.5
2.8	8.75 ± 0.30	8.5 ± 0.5	7.5 ± 0.5
3.0	9.50 ± 0.30	10.0 ± 0.5	9.5 ± 0.5
3.2	10.75 ± 0.30	11.5 ± 0.5	11.0 ± 0.5
3.7	11.30 ± 0.30	14.2 ± 0.5	13.0 ± 0.5
4.0	12.15 ± 0.30	13.5 ± 0.5	10.0 ± 0.5
5.0	12.30 ± 0.30	11.5 ± 0.5	9.5 ± 0.5
6.0	12.45 ± 0.30	8.0 ± 0.5	7.5 ± 0.5

**Figure 5.** Typical indentations for two different indenter diagonal orientations. (Load 100 N).

Study of the specimen containing 4.0 mol.% Sm₂O₃ by local Raman spectroscopy showed the presence of the monoclinic phase inside the indentation (Figure 6). This suggests the occurrence of the tetragonal to monoclinic phase transformation initiated by the mechanical loads during the indentation.

These experimental data are in agreement with X-ray phase analysis data for the specimens of different compositions. The crystals containing 2.0 and 2.8 mol.% Sm₂O₃ consist of the monoclinic ZrO₂ modification with a small quantity of the tetragonal phase. The monoclinic phase does not exhibit good mechanical parameters [30], and therefore these crystals have relatively low fracture toughness. The crystals containing 3.0 and 3.2 mol.% Sm₂O₃ retain a small quantity of the monoclinic phase, which is completely eliminated at 3.7 mol.% Sm₂O₃. The absence of the monoclinic phase in combination with the highest concentration of the transformable t phase seems to determine the highest fracture toughness of the crystals of these compositions. The following decline in the fracture toughness of the crystals with an increase in the Sm₂O₃ concentration within a range of 3.7–6.0 mol.% originates from a decrease in the content of the transformable t phase.

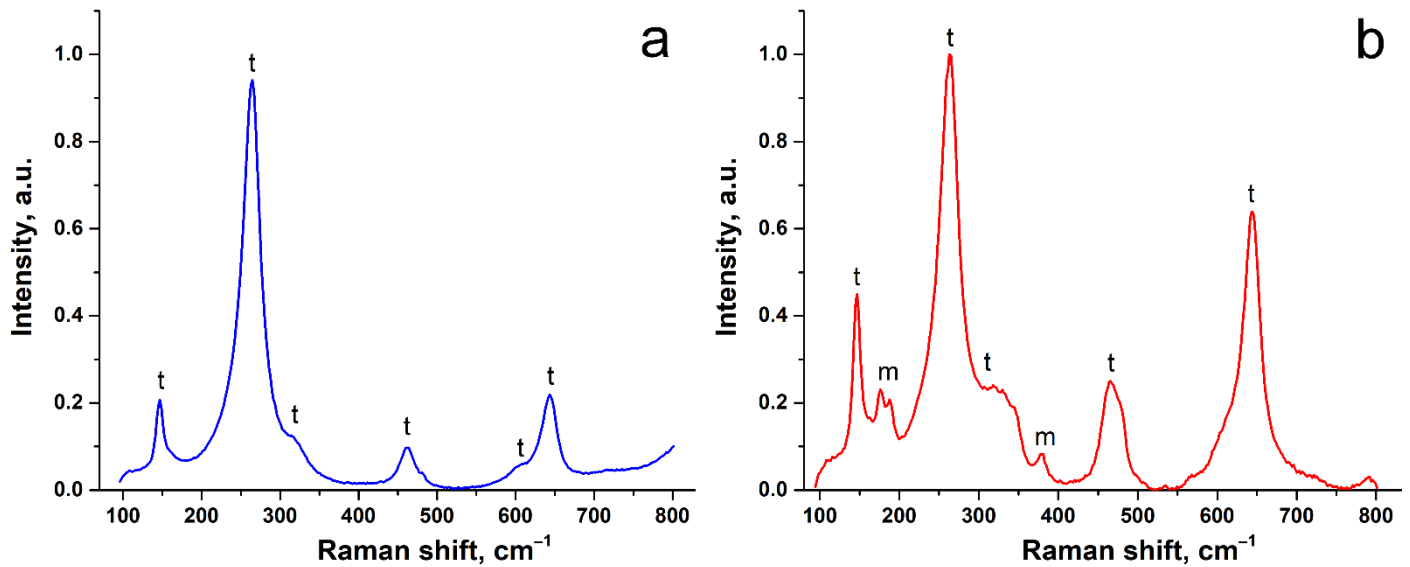


Figure 6. Raman spectra of $(\text{ZrO}_2)_{0.96}(\text{Sm}_2\text{O}_3)_{0.04}$ crystal: (a) near the indentation, (b) inside the indentation.

It is of interest to compare these experimental results with earlier data for $(\text{ZrO}_2)_{1-x}(\text{Y}_2\text{O}_3)_x$ [20] and $(\text{ZrO}_2)_{1-x}(\text{Gd}_2\text{O}_3)_x$ [21] crystals (Figure 7). This comparison seems to be justified since all the crystals were grown by directional melt crystallization under similar process conditions (crystallization and cooling rates and temperature regimes), and the measurement methods used were also the same.

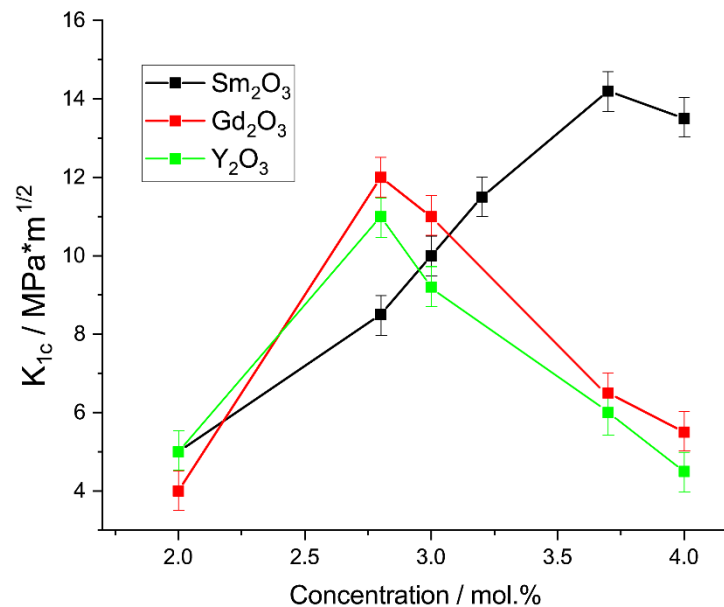


Figure 7. Fracture toughness of (1) $(\text{ZrO}_2)_{1-x}(\text{Sm}_2\text{O}_3)_x$, (2) $(\text{ZrO}_2)_{1-x}(\text{Y}_2\text{O}_3)_x$ and (3) $(\text{ZrO}_2)_{1-x}(\text{Gd}_2\text{O}_3)_x$ crystals as a function of stabilizing oxide concentration.

The concentration dependences of the fracture toughness of the $(\text{ZrO}_2)_{1-x}(\text{Y}_2\text{O}_3)_x$ and $(\text{ZrO}_2)_{1-x}(\text{Gd}_2\text{O}_3)_x$ crystals have similar patterns. The highest fracture toughness is observed at a Y_2O_3 or Gd_2O_3 content of 2.8 mol.%. At a comparable stabilizing oxide concentration, the fracture toughness of the $(\text{ZrO}_2)_{1-x}(\text{Gd}_2\text{O}_3)_x$ crystal proves to be higher than that of the $(\text{ZrO}_2)_{1-x}(\text{Y}_2\text{O}_3)_x$ one. The concentration dependence of the fracture toughness of the $(\text{ZrO}_2)_{1-x}(\text{Sm}_2\text{O}_3)_x$ crystals also exhibits a peak, but it is shifted towards higher stabilizing oxide concentrations. The highest fracture toughness of the $(\text{ZrO}_2)_{1-x}(\text{Sm}_2\text{O}_3)_x$

crystals is higher than that of the $(\text{ZrO}_2)_{1-x}(\text{Gd}_2\text{O}_3)_x$ crystals, which is in turn higher than that of the $(\text{ZrO}_2)_{1-x}(\text{Y}_2\text{O}_3)_x$ ones. This dependence correlates well with the growth of the ionic radius in the sequence $R_{\text{Y}^{3+}} < R_{\text{Gd}^{3+}} < R_{\text{Sm}^{3+}}$.

4. Conclusions

$(\text{ZrO}_2)_{1-x}(\text{Sm}_2\text{O}_3)_x$ crystals ($x = 0.02\text{--}0.06$) were grown using directional melt crystallization in a cold skull. A local Raman spectroscopic study of the crystals showed that, in some cases, the phase composition of the crystals changes along the crystal, probably because of a variable quantity of cations with a larger ionic radius being incorporated into the crystal lattice. Optical spectroscopy showed that Sm ions were incorporated into the ZrO_2 crystal lattice mainly in the form of Sm^{3+} . The evolution of the phase composition of the crystals depending on the Sm_2O_3 concentration was studied using X-ray phase analysis. The phase composition proved to change with an increase in the Sm_2O_3 concentration in the sequence $m \rightarrow m + t \rightarrow m + t + t' \rightarrow t + t'$. The monoclinic phase was completely eliminated at a concentration of $\text{Sm}_2\text{O}_3 \geq 3.7$ mol.%. The microhardness of the crystals grew monotonically with an increase in the Sm_2O_3 concentration, reaching 12.45 GPa for the $(\text{ZrO}_2)_{0.94}(\text{Sm}_2\text{O}_3)_{0.06}$ crystals. The highest fracture toughness of 14.2 $\text{MPa}\cdot\text{m}^{1/2}$ was observed in the crystals containing 3.7 mol.% Sm_2O_3 . The high fracture toughness of the crystals of this composition seems to originate from a combination of several factors: the highest concentration of the transformable t phase, and the high transformability and the absence of the monoclinic phase. A comparison of these experimental results with earlier data for $(\text{ZrO}_2)_{1-x}(\text{Y}_2\text{O}_3)_x$ and $(\text{ZrO}_2)_{1-x}(\text{Gd}_2\text{O}_3)_x$ crystals showed that the maximum fracture toughness increases with the ionic radius of the stabilizing oxide.

Author Contributions: Conceptualization, M.B., P.R., E.L. and N.T.; formal analysis, V.M., A.C. and N.S.; investigation, N.T., N.S. and F.M.; methodology, P.R.; resources, M.B., A.K., E.L., V.M. and N.T.; supervision, M.B. and E.L.; validation, P.R. and N.T.; visualization, F.M.; writing—review and editing, M.B. and P.R. All authors have read and agreed to the published version of the manuscript.

Funding: This research was funded by Russian Science Foundation, grant number 22-29-01220.

Conflicts of Interest: The authors declare no conflict of interest.

References

- Piconi, C.; Maccauro, G. Zirconia as a ceramic biomaterial. *Biomaterials* **1999**, *20*, 1–25. [[CrossRef](#)]
- Mahato, N.; Banerjee, A.; Gupta, A.; Omar, S.; Balani, K. Progress in material selection for solid oxide fuel cell technology: A review. *Prog. Mater. Sci.* **2015**, *72*, 141–337. [[CrossRef](#)]
- Vaßen, R.; Jarligo, M.O.; Steinke, T.; Mack, D.E.; Stöver, D. Overview on advanced thermal barrier coatings. *Surf. Coat. Technol.* **2010**, *205*, 938–942. [[CrossRef](#)]
- Chevalier, J.; Gremillard, L.; Virkar, A.V.; Clarke, D.R. The tetragonal-monoclinic transformation in zirconia: Lessons learned and future trends. *J. Am. Ceram. Soc.* **2009**, *92*, 1901–1920. [[CrossRef](#)]
- Heuer, A.H.; Rühle, M.; Marshall, D.B. On the Thermoelastic Martensitic Transformation in Tetragonal Zirconia. *J. Am. Ceram. Soc.* **1990**, *73*, 1084–1093. [[CrossRef](#)]
- Garvie, R.C.; Hannink, R.H.J.; Pascoe, R.T. Ceramic Steel? *Nature* **1975**, *258*, 703–704. [[CrossRef](#)]
- Li, Q.; Hao, X.; Gui, Y.; Qiu, H.; Ling, Y.; Zheng, H.; Omran, M.; Gao, L.; Chen, J.; Chen, G. Controlled sintering and phase transformation of yttria-doped tetragonal zirconia polycrystal material. *Ceram. Int.* **2021**, *47*, 27188–27194. [[CrossRef](#)]
- Yoshimura, M.; Yashima, M.; Noma, T.; Somiya, S. Formation of diffusionlessly transformed tetragonal phases by rapid quenching of melts in $\text{ZrO}_2\text{-RO}_{1.5}$ systems (R = rare earths). *J. Mater. Sci.* **1990**, *25*, 2011–2016. [[CrossRef](#)]
- Shi, Q.; Yuan, W.; Chao, X.; Zhu, Z. Phase stability, thermal conductivity and crystal growth behavior of RE_2O_3 (RE = La, Yb, Ce, Gd) co-doped Y_2O_3 stabilized ZrO_2 powder. *J. Sol. Gel Sci. Technol.* **2017**, *84*, 341–348. [[CrossRef](#)]
- Chen, D.; Wang, Q.; Liu, Y.; Ningm, X. Microstructure, thermal characteristics, and thermal cycling behavior of the ternary rare earth oxides (La_2O_3 , Gd_2O_3 , and Yb_2O_3) co-doped YSZ coatings. *Surf. Coat. Technol.* **2020**, *403*, 126387. [[CrossRef](#)]
- Donat, L.; Osswald, B.; Kern, F. 1Yb-2Sm-TZP, a new co-stabilized zirconia material with high toughness and low temperature degradation resistance. *J. Eur. Ceram. Soc.* **2022**, *in press*. [[CrossRef](#)]
- Huang, W.; Qiu, H.; Zhang, Y.; Zhang, F.; Gao, L.; Omran, M.; Chen, G. Microstructure and phase transformation behavior of $\text{Al}_2\text{O}_3\text{-ZrO}_2$ under microwave sintering. *Ceram. Int.* **2022**, *in press*. [[CrossRef](#)]
- Ling, Y.; Li, Q.; Zheng, H.; Omran, M.; Gao, L.; Chen, J.; Chen, G. Optimisation on the stability of CaO-doped partially stabilised zirconia by microwave heating. *Ceram. Int.* **2021**, *47*, 8067–8074. [[CrossRef](#)]

14. Li, Q.; Ling, Y.; Zheng, H.; Chen, G.; Chen, J.; Koppala, S.; Jiang, Q.; Li, K.; Omran, M.; Gao, L. Phase microstructure and morphology evolution of MgO-PSZ ceramics during the microwave sintering process. *Ceram. Int.* **2021**, *47*, 15849–15858. [[CrossRef](#)]
15. Yashima, M.; Ohtake, K.; Kakihana, M.; Arashi, H.; Yoshimura, M. Determination of tetragonal-cubic phase boundary of $Zr_{1-x}R_xO_{2-x/2}$ (R= Nd, Sm, Y, Er and Yb) by Raman scattering. *J. Phys. Chem. Solids* **1996**, *57*, 17–24. [[CrossRef](#)]
16. Wang, C.; Zinkevich, M.; Aldinger, F. Phase diagrams and thermodynamics of rare-earth-doped zirconia ceramics. *Pure Appl. Chem.* **2007**, *79*, 1731–1753. [[CrossRef](#)]
17. Katamura, J.; Seri, T.; Sakuma, T. The Cubic-Tetragonal Phase Equilibria in the ZrO_2 - R_2O_3 (R=Y, Gd, Sm, Nd) Systems. *J. Phase Equilibria* **1995**, *16*, 315–319. [[CrossRef](#)]
18. Scott, H.G. Phase Relationships in the Yttria-rich Part of the Yttria-Zirconia System. *J. Mater. Sci.* **1977**, *12*, 311–316. [[CrossRef](#)]
19. Andrievskaya, E.R. Phase equilibria in the refractory oxide systems of zirconia, hafnia and yttria with rare-earth oxides. *J. Eur. Ceram. Soc.* **2008**, *28*, 2363–2388. [[CrossRef](#)]
20. Borik, M.A.; Bublik, V.T.; Kulebyakin, A.V.; Lomonova, E.E.; Milovich, F.O.; Myzina, V.A.; Osiko, V.V.; Seryakov, S.V.; Tabachkova, N.Y. Change in the phase composition, structure and mechanical properties of directed melt crystallised partially stabilised zirconia crystals depending on the concentration of Y_2O_3 . *J. Eur. Ceram. Soc.* **2015**, *35*, 1889–1894. [[CrossRef](#)]
21. Borik, M.A.; Chislov, A.S.; Kulebyakin, A.V.; Lomonova, E.E.; Milovich, F.O.; Myzina, V.A.; Ryabochkina, P.A.; Sidorova, N.V.; Tabachkova, N.Y. Effect of heat treatment on the structure and mechanical properties of partially gadolinia-stabilized zirconia crystals. *J. Asian Ceram. Soc.* **2021**, *9*, 559–569. [[CrossRef](#)]
22. Borik, M.A.; Borichevskij, V.P.; Bublik, V.T.; Kulebyakin, A.V.; Lomonova, E.E.; Milovich, F.O.; Myzina, V.A.; Ryabochkina, P.A.; Sidorova, N.V.; Tabachkova, N.Y. Anisotropy of the mechanical properties and features of the tetragonal to monoclinic transition in partially stabilized zirconia crystals. *J. Alloy Compd.* **2019**, *792*, 1255–1260. [[CrossRef](#)]
23. Osiko, V.V.; Borik, M.A.; Lomonova, E.E. Synthesis of Refractory Materials by Skull Melting Technique. In *Springer Handbook of Crystal Growth*; Springer Science and Business Media LLC: Berlin/Heidelberg, Germany, 2010; pp. 433–477.
24. Niihara, K.A. A fracture mechanics analysis of indentation-induced Palmqvist crack in ceramics. *J. Mater. Sci. Lett.* **1983**, *2*, 2221–2223. [[CrossRef](#)]
25. Borik, M.A.; Lomonova, E.E.; Osiko, V.V.; Panov, V.A.; Porodinkov, O.E.; Vishnyakova, M.A.; Voron'ko, Y.K.; Voronov, V.V. Partially stabilized zirconia single crystals: Growth from the melt and investigation of the properties. *J. Cryst. Growth* **2005**, *275*, e2173–e2179. [[CrossRef](#)]
26. Hemberger, Y.; Wichtner, N.; Berthold, C.; Nickel, K.G. Quantification of yttria in stabilized zirconia by Raman spectroscopy. *Int. J. Appl. Ceram. Technol.* **2016**, *13*, 116–124. [[CrossRef](#)]
27. Shih, H.R.; Chang, Y.S. Structure and photoluminescence properties of Sm^{3+} ion-doped $YInGe_2O_7$ phosphor. *Materials* **2017**, *10*, 779. [[CrossRef](#)] [[PubMed](#)]
28. Hulliger, J. Crystal chemistry and crystal growth of optical materials. *Chimia* **2001**, *55*, 1025–1028. [[CrossRef](#)]
29. Liu, Z.; Stevens-Kalceff, M.; Riesen, H. Photoluminescence and cathodoluminescence properties of nanocrystalline BaFCl: Sm^{3+} X-ray storage phosphor. *J. Phys. Chem. C* **2012**, *116*, 8322–8331. [[CrossRef](#)]
30. Chan, S.K.; Fang, Y.; Grimsditch, M.; Li, Z.; Nevitt, M.V.; Robertson, W.M.; Zouboulis, E.S. Temperature dependence of the elastic moduli of monoclinic zirconia. *J. Am. Ceram. Soc.* **1991**, *74*, 1742–1744. [[CrossRef](#)]